Topics in Catalysis (2020) 63:750–761
https://doi.org/10.1007/s11244-020-01246-7

ORIGINAL PAPER

$Pd_3Ag(111)$ as a Model System for Hydrogen Separation Membranes: Combined Effects of CO Adsorption and Surface Termination on the Activation of Molecular Hydrogen

Ingeborg-Helene Svenum[1,2] · Jeffrey A. Herron[3] · Manos Mavrikakis[3] · Hilde J. Venvik[1]

Published online: 2 March 2020

Abstract
The co-adsorption of hydrogen and carbon monoxide on $Pd_3Ag(111)$ alloy surfaces has been studied as a model system for Pd-Ag alloys in membrane and catalysis applications using periodic density functional theory calculations (PW91-GGA). We explored the effects of Pd–Ag surface composition, since segregation of silver towards and away from the surface has been suggested to explain the experimentally observed changes in H_2 activation, CO inhibition and reactivity. We found that CO pre-adsorbed on the surface weakens the adsorption of H on $Pd_3Ag(111)$ alloy surfaces irrespective of whether the surface termination corresponds to the bulk Pd_3Ag composition, or is purely Pd-terminated. A higher coverage of H with CO present is obtained for the Pd-terminated surface; this surface also exhibits a larger range of chemical potentials for co-adsorbed hydrogen and CO. The barrier for H_2 activation increases with increasing CO coverage, but the surface composition has the largest impact on H_2 activation at intermediate CO coverage. The results imply that Pd-based membranes with typically ~ 23 wt% Ag are less prone to CO poisoning if the surface becomes Pd-terminated.

Keywords Palladium · Silver · Hydrogen · Carbon monoxide · Adsorption

1 Introduction

Palladium and its alloys are important because of their catalytic properties in hydrogenation, oxidation and other reactions. Moreover, the application of Pd in membranes for hydrogen separation is being developed [1, 2]. Pd has been alloyed with Ag in order to (1) enhance the catalytic activity by moderating the bond strength of adsorbed species [3, 4], or (2) to suppress the transition between different hydride phases in membranes or catalysts under hydrogen exposure [5–7]. The structure, composition and electronic properties of the Pd–Ag alloy surface are important in this respect, but the surface and sub-surface composition will also be affected by the segregation phenomena induced by changes in the reactive environment [8]. Understanding the energetics for adsorption of relevant atomic and molecular species as well as the segregation behavior of Pd–Ag alloys, and how these mutually affect each other, is therefore important.

The interaction of $CO + H_2$ with $Pd_{1-x}Ag_x$ surfaces is of particular relevance to membrane separation of hydrogen produced from carbon containing feedstock (natural gas, biomass or coal), as well as CO hydrogenation catalysis and the electro-oxidation of alcohols [9, 10]. We have long been involved in experimental work on thin, polycrystalline (1–10 µm) Pd alloy membranes, that may enable highly efficient separation of hydrogen from mixtures containing CO, CO_2, H_2O and CH_4; essentially also allowing a CO_2 rich retentate on the high-pressure side that is suitable for CO_2 capture and sequestration (CCS) [11]. Due to the low thickness and fabrication by sputtering that allows elimination of bulk and gas phase transport limitations in the membrane separation configuration, the effect of surface phenomena becomes more apparent. Depending on the process conditions as well as the thickness, CO may inhibit H_2 permeation through the Pd-based membranes [12–14]. We previously found, however, that the CO inhibition effect on ~ 3 µm thin

✉ Ingeborg-Helene Svenum
Ingeborg-Helene.Svenum@sintef.no

1 Deparment of Chemical Engineering, Norwegian University of Science and Technology, 7491 Trondheim, Norway

2 SINTEF Industry, 7465 Trondheim, Norway

3 Department of Chemical and Biological Engineering, University of Wisconsin-Madison, Madison, Wisconsin 53706, USA

PdAg membranes could be largely reduced by first exposing the membranes to air at 573 K [15]. This procedure involves the formation of a PdO layer in the surface region, and while this oxide is readily reduced upon subsequent exposure to H_2, the enhanced permeation remains for the duration of the experiments (up to 85 days) [16]. Segregation of Pd to the surface has been suggested to contribute to the reduced inhibition effect towards CO [17, 18], in addition to surface roughening [18–22] and removal of impurities [23, 24].

Studies of hydrogen and CO adsorption on metal surfaces with controlled structure and composition has yielded information relevant to many industrial catalytic processes. For Pd and PdAg alloys, the interaction of H and CO has been investigated with a variety of different experimental techniques including low energy electron diffraction (LEED) [25–31], temperature desorption techniques [29–34], photoemission spectroscopy (PES) [35–40], and scanning tunneling microscopy (STM) [41–43]. Despite that most such investigations have been performed under ultra-high vacuum conditions in order to preserve information regarding structural, electronic, energetic, and vibrational properties, this has enabled significant insight relevant to catalyst and membrane applications. Recently, in-situ near ambient pressure photoelectron spectroscopy (NAP-PES) has opened up the possibility to investigate the reactivity and follow changes in the surface chemistry at reactant pressures more representative of the actual working conditions of a catalyst [44–48]. In addition, theoretical studies based on density functional theory (DFT) [17, 49–59] are increasingly complementing and facilitating the experimental interpretation.

H_2 adsorbs dissociatively on Pd(100) and Pd(111) single crystal surfaces [60–63], and H occupies hollow sites on both surfaces forming different adsorption structures depending on the coverage [26]. Hydrogen also readily absorbs in the subsurface of Pd [42, 49, 55]; the very property that makes Pd attractive as a membrane material. Pd-Ag alloy surfaces are predicted to behave similarly to Pd with respect to hydrogen, with H preferentially occupying hollow sites independent of surface coverage [17, 50, 64]. Compared to Pd(111), however, hydrogen dissolves more easily into the subsurface of PdAg(111) and the desorption of H occurs at a higher temperature [31]. It has been observed experimentally that CO adsorbs molecularly in an upright configuration on Pd(111) where different ordered structures may stabilize depending on the CO coverage [29, 41, 65, 66]. For Pd–Ag alloy surfaces, no ordered CO overlayer structures have been observed. CO generally favors adsorption sites with high Pd coordination on Pd–Ag surfaces [31, 67], which is in agreement with DFT calculations [17, 54].

Using periodic DFT calculations, we have previously investigated the H_2/CO/O_2 adsorbate system over $Pd_3Ag(111)$ model systems in order to better understand how the adsorption energetics and the segregation behavior are mutually affected. Our previous theoretical investigation examined the individual adsorbates (H_2, CO, O_2) on different $Pd_3Ag(111)$ terminations, including effects of coverage [17]. These calculations were consistent with other experimental and theoretical studies establishing that, in absence of adsorbates (i.e. vacuum/inert atmosphere), the thermodynamically stable surface is Ag rich [68–76]. We further showed, however, that Pd is energetically favored in the topmost layer upon adsorption of H, O, or CO. This would make a Pd–Ag alloy surface Pd-rich at the corresponding saturation coverage if the conditions simultaneously favor the segregation kinetics. In the present work, we examine CO and H_2 co-adsorption, more specifically the effect of CO adsorption on the adsorption and dissociation of H_2 on Pd–Ag alloy surfaces. A bulk-terminated $Pd_3Ag(111)$ surface is compared with a Pd-terminated Pd_3Ag alloy. Different compositions of Pd and Ag in the surface are considered in order to investigate the effect of segregation under reactive conditions and the dissociation of H_2 is explored as a function of increasing CO coverage. Lastly, we constructed a phase diagram as a function of CO and H_2 chemical potentials evaluating the coverage at relevant temperature and pressure conditions.

2 Methodology

The calculations investigating the co-adsorption of H and CO on a Pd- and a bulk-terminated $Pd_3Ag(111)$ surface, were performed using periodic DFT as implemented in DACAPO [77, 78]. The exchange-correlation energy and potential are described by the generalized gradient approximation (GGA-PW91) [79, 80], and the ionic cores were described by ultrasoft Vanderbilt pseudopotentials [81]. The Kohn–Sham wave functions were expanded in a plane-wave basis with an energy cutoff of 400 eV, and the surface Brillouin zone was sampled with 18 special k-points [82].

The $Pd_3Ag(111)$ alloy surfaces, where Pd_3Ag possesses a fcc $L1_2$-like structure, are modeled using a six layer slab with a (2×2) surface unit cell. A vacuum layer corresponding to six atomic layers was applied between successive images of the slab. The optimized bulk lattice constant for Pd_3Ag is calculated to be 4.014 Å [17], in reasonable agreement with the experimental value of 3.926 Å [83]. The four topmost layers were free to relax without any restrictions imposed during structural optimization, whereas the two bottom layers were fixed to the lattice structure of the bulk. The geometries were relaxed until the force components on each atom were less than 0.02 eV/Å, and the convergence criterion for the electronic self-consistent loop was set to 10^{-5} eV. The bulk-terminated surface has 25% Ag and 75% Pd in the surface and Ag evenly distributed throughout the slab. The overall Pd:Ag ratio of the slab is maintained at 3:1 for the Pd-terminated

surface, for which the Ag atom in the topmost layer is exchanged with a second layer Pd atom. H and CO adsorption and co-adsorption is investigated on both surfaces at different H/CO ratios. Subsurface hydrogen is not included in this study. Adsorption is allowed on one side of the slab only, and the electrostatic potential is adjusted accordingly [84, 85]. The many possible co-adsorbed structures have been rigorously examined. The differential binding energy, BE_{diff}, was defined as:

$$BE_{diff} = E_{N_{Ads}/surf} - \left(E_{(N_{Ads}-1)/surf} + E_{Ads}\right) \quad (1)$$

$E_{N_{Ads}/surf}$ is the total energy of the adsorbate-substrate system with N_{Ads} adsorbates, and $E_{(N_{Ads}-1)/surf}$ is the total energy of the adsorbate-substrate system with $(N_{Ads} - 1)$ adsorbates. E_{surf} $(N_{Ads} - 1 = 0)$ is the total energy of the clean Pd-Ag surface and E_{Ads} is the total energy of a gas-phase CO molecule or H atom. For the co-adsorbed system, E_{surf} corresponds to the surface with CO pre-adsorbed. Adsorption is energetically favorable when BE_{diff} is negative. Predicted saturation coverage of H is reached when BE_{diff} is below the value of the bond energy of H_2 per atom.

Climbing image nudged elastic band (CI-NEB) calculations [86] were used to calculate activation energy barriers for H_2 dissociation with increasing amount of CO pre-adsorbed. 7 or 11 images were typically used for the CI-NEB calculations, and the calculations were optimized yielding forces below 0.05 eV/Å. Transition states were verified using vibrational analysis resulting in a single imaginary frequency.

Surface phase diagrams were constructed to identify the most stable CO and/or H adsorption structures as a function of reaction conditions. The surfaces were assumed to be in thermodynamic equilibrium with gas phase CO and H_2 following the constrained equilibrium approach [87–89]. In this approach, the species are not allowed to react with each other and the Gibbs free energy for adsorption, ΔG^{ads}, is expressed by

$$\Delta G^{ads} = -\frac{1}{A}\left[G_{H,CO/surf} - G_{surf} - N_H\mu_H - N_{CO}\mu_{CO}\right] \quad (2)$$

where A is the surface area, $G_{H,CO/surf}$ is the Gibbs free energy for the surface with N_H hydrogen and N_{CO} CO species adsorbed. G_{surf} is the Gibbs free energy for the surface in the absence of any adsorbates. μ_H and μ_{CO} represent the chemical potential of the two gas phase reservoirs of hydrogen and CO, respectively. Assuming ideal gas, they can be expressed as a function of temperature and pressure:

$$\mu_H(T, p_{H_2}) = \frac{1}{2}\left[E_{H_2} + \tilde{\mu}_{H_2}(T, p^0) + k_B T \ln\frac{p_{H_2}}{p^0}\right] = \frac{1}{2}\left(E_{H_2} + \Delta\mu_{H_2}\right) \quad (3)$$

and

$$\mu_{CO}(T, p_{CO}) = E_{CO} + \tilde{\mu}_{CO}(T, p^0) + k_B T \ln\frac{p_{CO}}{p^0} = E_{CO} + \Delta\mu_{CO} \quad (4)$$

where p^0 is the standard pressure. The chemical potential of molecular and atomic hydrogen is related by $\mu_H = 1/2 \times \mu_{H_2}$. The chemical potentials of H_2 and CO at standard pressure, $\tilde{\mu}_{H_2}(T, p^0)$ and $\tilde{\mu}_{CO}(T, p^0)$ are evaluated using the NIST-JANAF thermochemical database [90]. E_{H_2} and E_{CO} are the total energies of the gas-phase H_2 and CO molecules, respectively. ΔG^{ads} can be approximated to

$$\Delta G^{ads} \approx \frac{1}{A}\left[-BE_{ave} + N_H\Delta\mu_H + N_{CO}\Delta\mu_{CO}\right] \quad (5)$$

BE_{ave} is the average binding energy for H and CO given by

$$BE_{ave} = \left(E_{H,CO/surf} - E_{surf} - \frac{N_H}{2}E_{H_2} - N_{CO}E_{CO}\right) \quad (6)$$

where $E_{H,CO/surf}$ is the total energy of the co-adsorbed system. The average binding energy is corrected for zero-point energies.

3 Results and Discussion

3.1 Adsorption and Activation on Bulk-Terminated $Pd_3Ag(111)$

For the H + CO co-adsorbed system, we consider changes in the adsorption energetics upon hydrogen adsorption on a bulk-terminated $Pd_3Ag(111)$ surface with increasing amounts of CO pre-adsorbed. The differential binding energy of hydrogen for increasing CO pre-coverage is shown in Fig. 1. We have previously published the coverage dependent interaction of H or CO alone with differently terminated $Pd_3Ag(111)$ surfaces [17]. Results from that study, representing the starting point for the current study, are included here. Table 1 summarizes the optimized adsorption geometries for different coverages of either H or CO.

In the absence of adsorbed CO, the predicted hydrogen saturation coverage for $Pd_3Ag(111)$ is 1.00 ML, since the differential binding energy becomes endothermic relative to H_2 in the gas phase (1/2 E_{H_2}) above this coverage (see lower curve of Fig. 1). The differential binding energy of 0.25 ML H is − 2.85 eV in a fcc site made up by Pd. The preference for the fcc site found here is consistent with predictions for Pd(111) where the fcc is generally favored over the hcp site by around 0.05 eV [50, 53, 58, 59]. With increasing coverage, H atoms populate hollow sites with the highest Pd concentration available, favoring fcc sites in agreement with previous studies [17, 50, 64]. Figure 2a illustrates the $Pd_3Ag(111)$ surface at the predicted H saturation coverage.

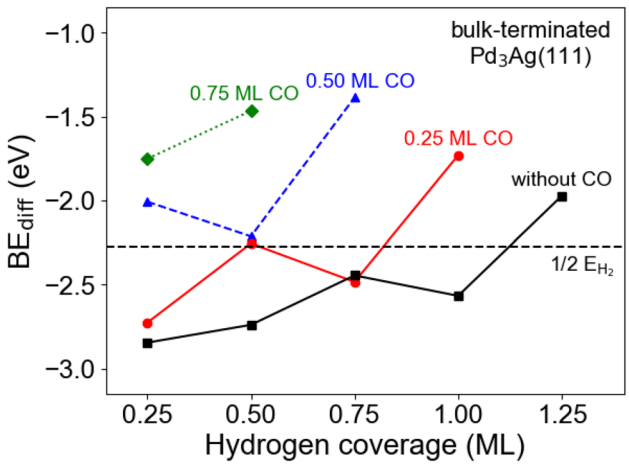

Fig. 1 Differential binding energy for H as a function of coverage on bulk-terminated $Pd_3Ag(111)$ surfaces without and with increasing amount of CO pre-adsorbed. The dotted horizontal line represents the calculated bond energy of H_2 (g) per atom

Table 1 Preferred adsorption sites and differential binding energies of CO and H adsorbed individually on the bulk-terminated Pd3Ag(111) surface

Adsorbate	Coverage (ML)	Sites	BE_{diff} (eV)
H	0.25	fcc_{3Pd}	− 2.85
	0.50	$fcc_{3Pd}+hcp_{3Pd}$	− 2.74
	0.75	$fcc_{3Pd}+2\times fcc_{2PdAg}$	− 2.45
	1.00	$fcc_{3Pd}+3\times fcc_{2PdAg}$	− 2.57
CO	0.25	fcc_{3Pd}	− 2.01
	0.50	$fcc_{3Pd}+hcp_{3Pd}$	− 1.63
	0.75	$2\times br_{Pd}+top_{Pd}$	− 0.26

The index after the different sites, fcc, hcp, bridge (br) and top, refers to the local composition of the corresponding site in the surface layer, eg. fcc_{3Pd} describes a fcc site consisting of three Pd atoms

In sites of mixed composition, e.g. an fcc site comprising 2 Pd atoms and 1 Ag atom in the top layer (here denoted fcc_{2PdAg}), the H atom is displaced toward surface Pd atoms and away from Ag. Overall, H atoms repel each other when adsorbed on this surface and, on average, the differential binding energy of H decreases in magnitude as the H coverage increases.

In the absence of adsorbed H, CO occupies the fcc_{3Pd} site on the bulk-terminated $Pd_3Ag(111)$ at 0.25 ML with a differential binding energy of − 2.01 eV, similar to energies obtained for other Pd-based surfaces [53, 54, 91]. Hollow sites (fcc and hcp) made up by Pd alone are preferred on this surface at 0.50 ML, while CO prefers less coordinated sites over hollow sites with mixed Pd–Ag composition above this coverage. Adsorbed CO exhibits considerable repulsive interactions as the differential binding energy increases by 0.38 eV between 0.25 and 0.50 ML. At the saturation coverage (0.75 ML) depicted in Fig. 2b, the three CO molecules in the unit cell occupy one Pd top site and two Pd–Pd bridge sites (Table 1). The CO molecules in the latter positions are shifted towards the hollow site with the O atom tilted away from the CO in the top site (towards the surface Ag atom).

As shown in Fig. 1, the adsorption energetics of hydrogen is significantly influenced by the presence of adsorbed CO. Adding 0.25 ML H to a surface containing 0.25 ML CO makes the adsorption of H 0.12 eV less stable; CO, then, occupies the Pd-coordinated fcc site while H goes to the corresponding hcp site, in a similar configuration as for 0.50 ML H or CO alone. At higher H coverage, CO persists in occupying the fcc_{3Pd} site while H attains fcc sites of mixed Pd–Ag composition. However, with 0.25 ML CO the differential binding energy of H is more negative at 0.75 ML compared to 0.50 ML H. A similar rearrangement effect exists for hydrogen adsorption alone upon increasing the coverage from 0.75 ML to 1.00 ML H and can be ascribed to the heterogeneity of the surface. Up to a total coverage of 0.5 ML H (no CO), hollow sites consisting of only Pd (fcc and hcp) are occupied, whereas only fcc sites become occupied at 0.75 ML hydrogen. In this case, two out of three sites have mixed composition, and this leads to significant destabilization caused by surface Ag atoms. Upon increasing the coverage to 1.00 ML in total, the remaining fcc sites become populated. Nevertheless, and in agreement with experimental findings [92, 93], adsorption sites occupied by CO remain inaccessible to H and the predicted hydrogen saturation coverage is reduced to 0.75 ML when 0.25 ML CO is pre-adsorbed.

Adsorption of hydrogen is not energetically favorable upon increasing the CO pre-coverage beyond 0.25 ML. The more positive differential BE signifies a rather strong repulsive interaction between the adsorbed species resulting in weaker bonding of hydrogen to the surface. Also, as the total CO + H coverage increases, a reconfiguration of preferred sites is observed, e.g. while CO is situated in a fcc and a hcp hollow site at 0.50 ML, the hcp bonded CO gains 0.45 eV by moving to a Pd–Pd bridge site upon hydrogen addition. H persists in the fcc hollow site, but in total, this rearrangement makes the 0.50 ML CO + 0.50 ML H configuration nearly thermoneutral with respect to H_2 (g) (Fig. 1).

As previously discussed, the presence of CO is also anticipated to affect the activation of H_2 on Pd based surfaces. First, we have considered H_2 dissociation on the clean and CO pre-covered $Pd_3Ag(111)$ surfaces up 0.75 ML CO. H_2 was initially placed above the surface with the H_2 bond parallel to the surface. Hydrogen dissociation relative to the most energetically stable CO adsorption structures was explored using CI-NEB calculations, and the energy profiles for dissociation relative to the gas phase are shown in Fig. 3. As expected, the dissociation of H_2 is non-activated

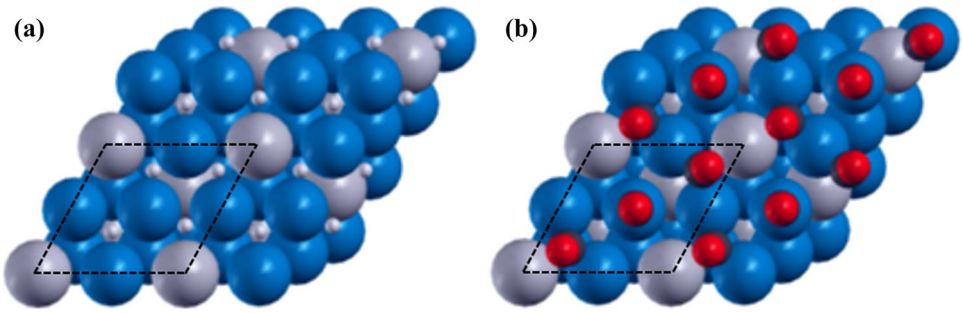

Fig. 2 Illustration of the bulk $Pd_3Ag(111)$ with the predicted saturation adsorption structures of **a** H (1.00 ML) and **b** CO (0.75 ML). No co-adsorption of H and CO is considered in this case. The (2×2) unit cell is outlined with dashed lines. Atoms are colored as follows: Pd—blue, Ag—grey, H—white, C—black, O—red

in the absence of CO. Paths without a barrier are found in Pd rich areas; between two fcc sites over a Pd–Pd bridge site or between one fcc and one hcp site. This agrees well with previous theoretical calculations for H_2 dissociation on Pd(111) [52, 94] and $Pd_3Ag(111)$ [95]. For the latter, it was reported that the activation energy barrier increased for dissociation paths close to surface Ag atoms. Clean Ag is inert towards H_2 dissociation [96–98], with barriers over Ag(111) calculated at 1.04 eV or higher [99–101]. Hydrogen dissociation would thus become difficult in Ag-rich areas of $Pd_{1-x}Ag_x(111)$ surfaces.

The activation energy barrier for H_2 dissociation becomes 0.04 eV when 0.25 ML CO is pre-adsorbed, with a preferred path that is well separated from the adsorbed CO molecule, i.e. over a Pd–Pd bridge site between fcc_{2PdAg} and hcp_{3Pd} sites. We conclude that low CO coverage has minor influence on H_2 dissociation, but the final dissociated state becomes less stable relative to adsorption on the surface with no CO pre-adsorbed (Fig. 3). Increasing the CO coverage to 0.50 ML leads to an activation energy barrier for H_2 dissociation of 0.94 eV, with the final state becoming endothermic with respect to H_2 (g). When 0.75 ML of CO is pre-adsorbed on the surface, corresponding to the CO-saturation coverage, H_2 dissociation is characterized by an activation energy barrier of 1.67 eV. In addition to the increased barrier for H_2 dissociation, there is a repulsive interaction between the approaching H_2 molecule and the pre-adsorbed CO molecule(s). Typically, CO is tilted away and/or moved to a different site during the dissociation process. This is more evident at higher CO coverage.

3.2 Adsorption and Activation on Pd-Terminated $Pd_3Ag(111)$

The differential binding energy of H on the Pd-terminated $Pd_3Ag(111)$ surface as a function of hydrogen coverage with increasing amount of CO pre-adsorbed is shown in Fig. 4. The lower curve represents hydrogen adsorption on the clean surface (no CO pre-adsorbed), with a predicted saturation coverage of 1.00 ML H. The differential binding energies of H or CO adsorbed alone on Pd-terminated $Pd_3Ag(111)$ are

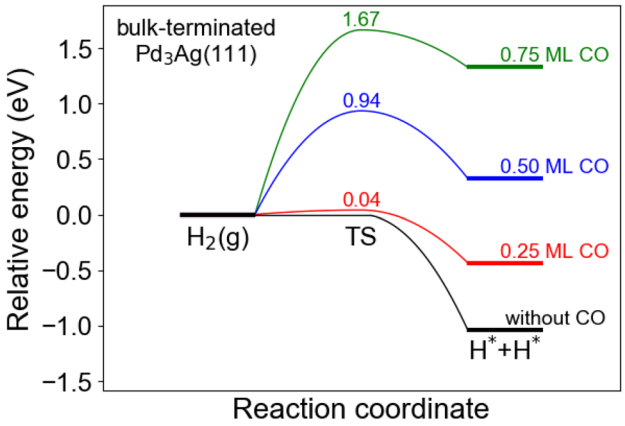

Fig. 3 Activation energy barrier for H_2 dissociation with increasing amount of CO pre-adsorbed on the bulk-terminated $Pd_3Ag(111)$ surface

listed in Table 2, and the preferred adsorption geometries at their predicted saturation coverages of 1.00 ML and 0.75 ML are illustrated in Fig. 5. The adsorption of H or CO on the Pd-terminated $Pd_3Ag(111)$ surface is similar to that of the bulk-terminated surface, in terms of both adsorbates displaying repulsive adsorbate interactions. Contrary to the bulk-terminated surface, however, the differential binding energy of H increases gradually since only fcc sites with the same composition are populated upon increasing coverage. The differential binding energies (Table 2) are more negative on the Pd-terminated surface compared to the bulk-terminated surface, except at 0.50 ML CO where the bonding is slightly stronger on the bulk-terminated surface. CO prefers to bind at fcc and hcp sites made up by Pd on both surfaces at 0.50 ML, with the concentration of Ag in the layer underneath causing the energy difference. The CO configuration differs between the two terminations at saturation coverage, with two hollow sites and one Pd top site occupied and an overall stronger interaction of CO on the Pd-terminated surface. This can be attributed to ensemble effects where the surface Ag atoms restrict the possibility for CO to occupy Pd hollow sites in addition to the top site in the case of the bulk-terminated Pd_3Ag surface. Hydrogen, in contrast, prefers fcc

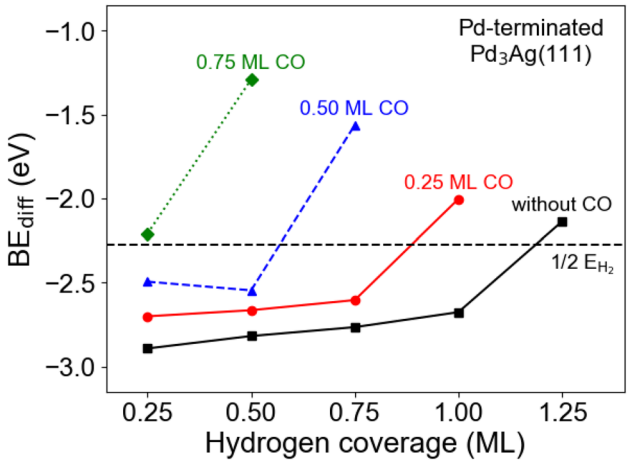

Fig. 4 Differential binding energy for H as a function of coverage on Pd-terminated $Pd_3Ag(111)$ surfaces without and with increasing amount of CO pre-adsorbed. The dotted horizontal line represents the calculated bond energy of H_2 (g) per atom

sites on Pd-terminated $Pd_3Ag(111)$ for all coverages listed in Table 2.

The energetics of hydrogen adsorption on this surface is strongly affected by the presence of pre-adsorbed CO, which destabilizes hydrogen. At low CO and H coverage (0.25 ML + 0.25 ML) the interactions of CO and H on the two surfaces are similar. However, as the coverages increase the species bind stronger to the Pd-terminated surface relative to the bulk-terminated $Pd_3Ag(111)$. As with the bulk-terminated $Pd_3Ag(111)$, in the presence of CO, the predicted hydrogen saturation coverage is also reduced on the Pd-terminated surface. In the absence of CO, the Pd-terminated surface can sustain a H saturation coverage of 1.00 ML (Fig. 4). That saturation coverage decreases to 0.75 ML H with 0.25 ML CO, as in the case of the bulk-terminated surface. But, while hydrogen adsorption is unfavorable on the bulk-terminated surface at higher CO coverage, 0.50 ML H is possible onto the 0.50 ML CO pre-covered Pd-terminated surface. H adsorption becomes endothermic only at the CO saturation coverage of 0.75 ML on the Pd-terminated surface.

The activation energy barriers for H_2 dissociation on the Pd-terminated $Pd_3Ag(111)$ surface as a function of

Table 2 Preferred adsorption sites and differential binding energies of CO and H adsorbed individually on the Pd-terminated Pd3Ag(111) surface

Adsorbate	Coverage (ML)	Sites	BE_{diff} (eV)
H	0.25	fcc	− 2.89
	0.50	2 × fcc	− 2.82
	0.75	3 × fcc	− 2.77
	1.00	4xfcc	− 2.68
CO	0.25	hcp	− 2.07
	0.50	fcc + hcp	− 1.46
	0.75	fcc + hcp + top	− 0.92

pre-adsorbed CO coverage are shown in Fig. 6. The dissociation is similar to that on the bulk-terminated surface in the absence of CO (non-activated) and at low CO coverage. With 0.25 ML CO pre-coverage there is a small activation energy barrier of 0.08 eV and the dissociation paths exhibiting the lowest barrier for both surface terminations are between two fcc sites or fcc and hcp over a Pd–Pd bridge site. The adsorbed hydrogen atoms are destabilized with CO present, but the destabilization is less than in the case of the bulk-terminated surface. Increasing the CO coverage to 0.5 ML on the Pd-terminated $Pd_3Ag(111)$ surface, leads to a H_2 dissociation barrier of 0.34 eV. It is at this intermediate CO coverage that the difference between bulk- and Pd-terminated $Pd_3Ag(111)$ is most significant, since hydrogen adsorption is still exothermic and the activation barrier is more than 0.6 eV lower when the surface is terminated by palladium only. At the CO saturation coverage of 0.75 ML, the H_2 dissociation barrier increases to 1.42 eV, which is 0.25 eV lower than that of the bulk-terminated surface.

Irrespective of termination, the calculations illustrate how the activation of hydrogen is affected by the presence of CO on the surface. Moreover, the two terminations studied here behave similarly for low and high CO coverage with respect to hydrogen dissociation. A transition from non-activated dissociation to a significant activation energy for increasing CO coverage is in agreement with studies of Pt(111) and Pt-terminated core-shell bimetallics

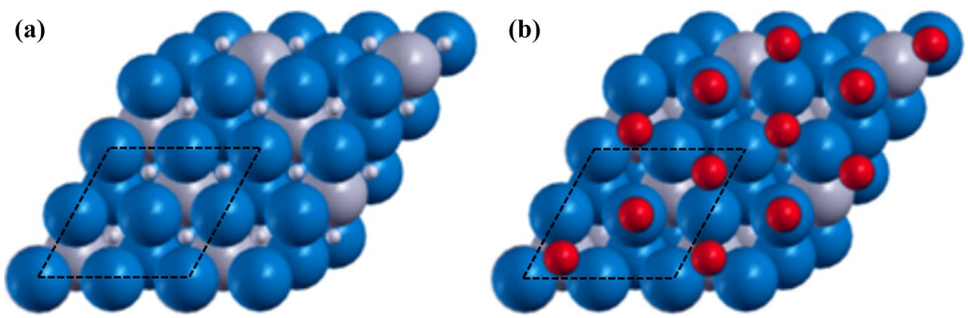

Fig. 5 Illustration of the Pd-terminated $Pd_3Ag(111)$ with the predicted saturation adsorption structures of **a** H (1.00 ML) and **b** CO (0.75 ML). The (2 × 2) unit cell is indicated by the black dashed lines. Atoms are colored as follows: Pd—blue, Ag—grey, H—white, C—black, O—red

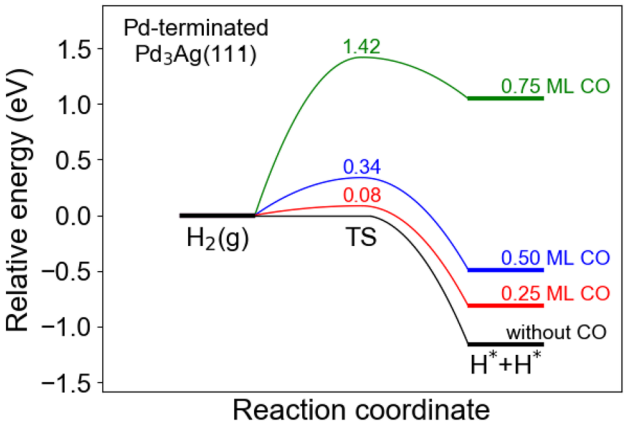

Fig. 6 Activation energy barrier for H_2 dissociation with increasing amount of CO pre-adsorbed on the Pd-terminated $Pd_3Ag(111)$ surface

by Nilekar and coworkers [102]. Our calculated activation energy barriers also agree qualitatively with studies of hydrogen dissociation over pure Pd membranes for CO coverages in the range 0–0.5 ML [103], but the semi-empirical quantification predicts somewhat lower barriers. Our findings indicate, however, that at intermediate CO coverage, a Pd-terminated Pd_3Ag surface is more reactive towards hydrogen than a bulk-terminated surface, due to the lower activation barrier.

3.3 Stability and Segregation Effects

To further evaluate the effect of CO on hydrogen adsorption we have constructed phase diagrams following the constrained equilibrium approach [87–89]. This allows examination of pressure and temperature effects in relation to hydrogen permeation and catalytic reaction experiments at application relevant conditions. ΔG^{ads} (Eq. 5) was evaluated on the two surface terminations studied for the relevant co-adsorbed configurations discussed above (0.25–1.00 ML H; 0.25–0.75 ML CO).

The phase diagrams in Fig. 7 show the most stable configurations of CO and H on the two surfaces as a function of the chemical potential of H_2 and CO. The secondary axes indicate the corresponding CO and H_2 partial pressures for two temperatures of potential interest for membrane separation and reactor applications, 300 K and 600 K [1]. For the lowest CO and H_2 chemical potentials the most stable configuration is the clean surface for both the bulk- and the Pd-terminated surface.

On the bulk-terminated $Pd_3Ag(111)$ surface, keeping the CO chemical potential low and increasing the hydrogen chemical potential, we found three stable hydrogen overlayer structures corresponding to H coverages of 0.25 ML, 0.50 ML and 1.00 ML starting at $\Delta\mu_{H_2}$ of − 1.08 eV, − 0.83 eV

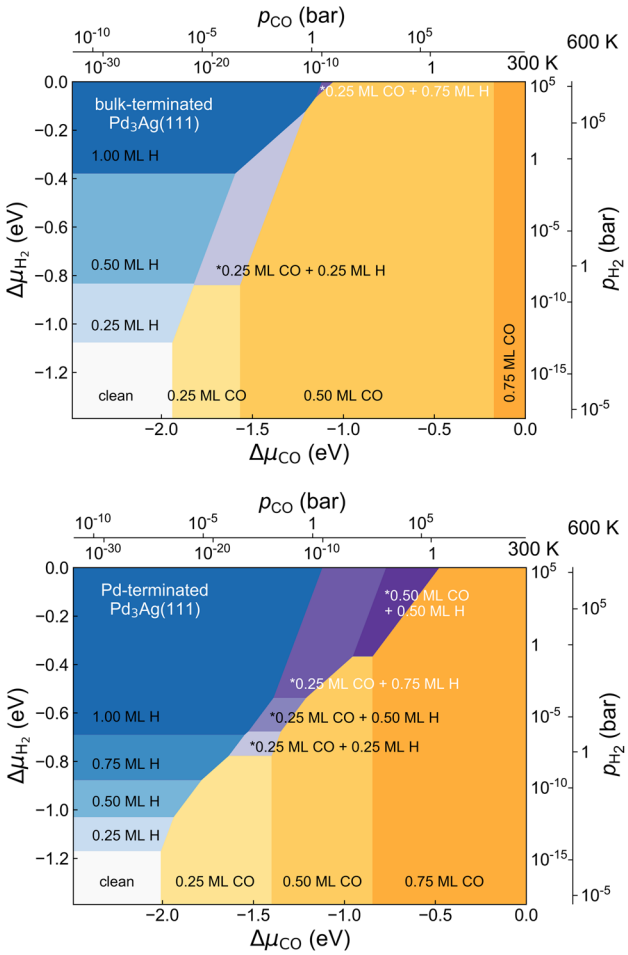

Fig. 7 Phase diagrams as a function of CO and hydrogen chemical potential for the bulk-terminated $Pd_3Ag(111)$ (upper panel) and the Pd-terminated $Pd_3Ag(111)$ (lower panel) surfaces. Secondary axes give pressure in H_2 and CO at two temperatures: 300 K (inner) and 600 K (outer) scales

and − 0.38 eV, respectively. 0.75 ML H is, however, found to be unstable for any $\Delta\mu_{H_2}$. This correlates well with the differential binding energy for 0.75 ML H (Fig. 1) being the energetically least favorable within the saturation range and suggesting a transition directly from a 0.50 ML to 1.00 ML covered surface. A similar non-sequential increase in hydrogen coverage has also been predicted for other surfaces; e.g. configurations corresponding to 0.50 ML and 1.00 ML (but not 0.75 ML) coverage were found stable on an (unreconstructed) Ni(111) surface [104].

On the Pd-terminated $Pd_3Ag(111)$ surface, however, the hydrogen coverage at low CO chemical potential increases by 0.25 ML increments up to saturation, see Fig. 7b, including the 0.75 ML phase, consistent with predictions for hydrogen on Pd(111) [105, 106]. The clean surface is preferred for H_2 chemical potentials lower than − 1.17 eV, with − 1.03 eV, − 0.88 eV and − 0.69 eV as threshold values for

the next phase transitions to increased hydrogen coverage upon increasing hydrogen chemical potential. The higher coverage at lower chemical potential reflects the stronger binding of H to the Pd-terminated surface compared to the bulk-terminated $Pd_3Ag(111)$ surface. The stronger interaction of hydrogen with the Pd-terminated surface implies segregation of Pd to the surface at temperatures of appreciable segregation kinetics. Thus, our previous conclusions from $Pd_3Ag(111)$ equilibrium ground state calculations predicting Pd-termination for hydrogen coverage exceeding 0.50 ML are not significantly altered [17].

The two $Pd_3Ag(111)$ surfaces studied behave similarly at low hydrogen chemical potential, upon increasing the CO chemical potential, with stable CO phases at 0.25, 0.50 and 0.75 ML. The 0.25 ML CO configuration becomes stable for CO chemical potentials of − 1.94 and − 2.01 eV for the bulk- and Pd-terminated surface, respectively. $\Delta\mu_{CO}$ of − 1.57 and − 1.40 eV is required for the two surfaces to become covered with 0.5 ML CO. The higher CO chemical potential obtained for the Pd-terminated surface relative to bulk-terminated $Pd_3Ag(111)$ can be explained by the Ag enrichment in the second topmost layer. The largest disparity is found for high CO chemical potentials, where the CO saturation coverage (0.75 ML) is reached at − 0.84 eV for the Pd-terminated surface, whereas the bulk-terminated surface maintains 0.5 ML CO up to $\Delta\mu_{CO}$ of − 0.17 eV. No ordered CO induced phases have been identified on Pd–Ag alloy surfaces from experimental investigations, likely reflecting the disordered nature of the Pd–Ag surface layer [31, 33, 107]. In contrast, several ordered structures have been observed for CO on Pd(111), including $(\sqrt{3}\times\sqrt{3})R30°$ (0.33 ML), c(4×2)-2CO (0.50 ML), and (2×2)-3CO (0.75 ML) [41, 65, 108], for which experimental $\Delta\mu_{CO}$ values of − 2.18, − 1.58 and − 0.71 eV, respectively, have been reported [65]. These values, together with values from previous theoretical work of about − 2.00, − 1.52 and − 0.69 eV [109], are relatively similar to the values predicted at similar coverages for the Pd-terminated surface studied here.

The phase diagrams in Fig. 7 suggest that hydrogen and CO may co-exist on both surfaces. For the bulk-terminated $Pd_3Ag(111)$ surface, configurations consisting of 0.25 ML CO plus 0.25 ML H and 0.25 ML CO plus 0.75 ML H are stable. The 0.25 ML CO with 0.75 ML H state is stable for a very limited range of CO and H chemical potentials. The Pd-terminated surface has a larger window of chemical potentials where adsorbed CO and H co-exist and overall higher coverages as already inferred from the differential binding energy considerations; see Sect. 3.2. Stable mixed adsorbed layers are obtained corresponding to coverages of 0.25 ML CO with 0.25, 0.50 and 0.75 ML H, and 0.50 ML CO with 0.50 ML H. Interestingly, even though the Pd-terminated surface binds both adsorbates stronger than the bulk-terminated, a higher CO chemical potential is generally required in order to transition into purely CO-covered phases on this surface for modest to high H_2 chemical potentials.

Hydrogen permeation applications are often targeted in the temperature range 500–700 K, at which the phase transition (α →β) in the Pd–Ag alloy is suppressed, the kinetics for hydrogen bulk diffusion is reasonably fast, and the integration into processes such as WGS and steam reforming is viable. From the analysis above it becomes apparent that, for the relevant range of CO and hydrogen partial pressures (20 ppm—20% and 10–80%, respectively, at 0.1–5 MPa), the coverages and phase changes predicted have importance. For example, the Pd-terminated surface exhibits larger variations in CO-partial pressures where hydrogen adsorption and activation are favorable than the bulk-terminated. Moreover, a higher CO partial pressure is required to shift into pure CO adsorption configurations at a specific temperature and hydrogen pressure.

Our results may help explain the performance of thin Pd–Ag alloy membranes, where the hydrogen transport may be impacted by surface phenomena. Specifically, it suggests that the increased permeation under pure hydrogen observed experimentally after oxidative treatment is correlated with Pd surface enrichment [18, 20, 21, 24, 110], since for a pure H_2 environment, presence of Ag in the topmost surface layer reduces the hydrogen adsorption energy as well as the coverage. The extent of segregation between Pd and Ag in differently prepared membranes, and specifically the distribution in the outmost surface layer may hence explain the performance observed under varying conditions and treatments of the membranes [15, 18, 20, 24]. The driving force for Pd to segregate towards the surface depends on both type of adsorbate and coverage [17], but diffusion in the bulk is kinetically controlled. This introduces considerable complexity in the dynamics of reactions over alloy surfaces. Fernandes et al. [45] recently explained decreased rates of reaction during CO oxidation over PdAg(100) observed at high temperature by reverse segregation effects (i.e. increased fraction of Ag termination upon increasing the temperature from ~ 525 to ~ 725 K) occurring due to decreased adsorbates coverage and facile segregation kinetics by a combined kinetic and first principles model. Further, our results generally agree with insights derived from studies of shallow versus deep hydrogenation over Pd-based catalysts, whereby alloying has been shown to be beneficial for moderating the binding strength of key intermediates/products thereby enhancing reaction selectivity towards shallow hydrogenation products [4, 111].

4 Conclusions

$Pd_3Ag(111)$ alloy surfaces have been studied as model systems for Pd–Ag membranes or catalysts. Through periodic DFT calculations, we have addressed the effect of surface

composition and segregation on co-adsorption of hydrogen and CO to understand the reactivity. At application relevant chemical potentials (p, T), we find that, for both Pd-terminated and bulk-terminated $Pd_3Ag(111)$ surfaces, adsorbed CO blocks hydrogen adsorption sites and weakens the binding of H, leading to a reduced hydrogen saturation coverage. The adsorption properties of the two surface terminations diverge at higher adsorbate coverage, where a higher coverage of H with CO present is obtained on the Pd-terminated surface. This surface also exhibits a wider range of chemical potentials for co-adsorbed mixtures of hydrogen and CO.

The surface composition of the bimetallic alloy furthermore influences the activation energy barrier for H_2 dissociation in the presence of pre-adsorbed CO. For both surface terminations, 0.25 ML CO leads to a minor activation energy barrier. The presence of Ag in the surface weakens the CO binding, but it still results in an activation energy barrier for H_2 dissociation on a CO saturated surface that makes H_2 dissociation unlikely. The most significant effect of surface composition is found at intermediate CO coverage (0.50 ML), with a considerably lower barrier for dissociative adsorption of H_2 for the Pd-terminated surface.

Under conditions relevant for hydrogen permeation and CO hydrogenation, our results imply that $Pd_3Ag(111)$ is less prone to CO poisoning if the surface becomes Pd-terminated. At the same time, the stronger binding of H and CO to pure Pd sites introduces a coverage dependent driving force for Pd segregation to the surface. This may explain some of the experimental observations related to Pd–Ag membrane performance enhancement under oxidation-reduction cycles.

Acknowledgements Open Access funding provided by NTNU Norwegian University of Science and Technology (incl St. Olavs Hospital - Trondheim University Hospital). The financial support from the Research Council of Norway through the ENERGIX (project no. 280903/E20) and KOSK (project no. 197709/V30) research programs, NTNU Thematic Strategic Area "Energy", and Equinor ASA through the NTNU-SINTEF Gas Technology Centre is thankfully acknowledged. J. A. H. and M. M. gratefully acknowledge financial support by the US Department of Energy, Office of Basic Energy Sciences, Division of Chemical Sciences (grant # DE-FG02-05ER15731). Computational work benefited from access to supercomputing resources provided by UNINETT Sigma2—the National Infrastructure for High Performance Computing and Data Storage in Norway (project no. nn9152k), and additional facilities at the National Energy Research Scientific Computing Center (NERSC), which is supported by the U.S. Department of Energy, Office of Science, under contract DE-AC02-05CH11231.

Compliance with Ethical Standards

Conflict of interest There are no known conflicts of Interest.

Ethical Approval The authors declare that the principles outlined in "Ethical Responsibilities of Authors" and "Authorship" sections of the Topics of Catalysis Submission Guidelines have been followed. All authors agreed with the content and gave explicit consent to submit.

Research Involving Human and Animal Partcipants The research has neither involved Human Participants nor Animals.

References

1. Bredesen R et al. (2011) Palladium-based Membranes in Hydrogen Production, In: E. Drioli and G. Barbieri (eds) Membrane engineering for the treatment of gases, Volume 2: gas-separation problems combined with membrane reactors.The Royal Society of Chemistry, pp 40–86
2. Peters TA, Bredesen R, Venvik HJ (2018) CHAPTER 6 Pd-based Membranes in hydrogen production: long-term stability and contaminant effects. In Membrane engineering for the treatment of gases: Volume 2: gas-separation issues combined with membrane reactors (2). The Royal Society of Chemistry, pp 177–211
3. Nørskov JK et al (2009) Towards the computational design of solid catalysts. Nat Chem 1(1):37–46
4. Sheth PA, Neurock M, Smith CM (2005) First-principles analysis of the effects of alloying Pd with Ag for the catalytic hydrogenation of acetylene–ethylene mixtures. J Phys Chem B 109(25):12449–12466
5. Knapton AG (1977) Palladium alloys for hydrogen diffusion membranes. Platin Met Rev 21:44
6. Fazle Kibria AKM, Sakamoto Y (2000) The effect of alloying of palladium with silver and rhodium on the hydrogen solubility, miscibility gap and hysteresis. Int J Hydrogen Energy 25(9):853–859
7. Grashoff GJ, Pilkington CE, Corti CW (1983) The purification of hydrogen. Platin Met Rev 27(4):157–169
8. Greeley J, Mavrikakis M (2004) Alloy catalysts designed from first principles. Nat Mater 3(11):810–815
9. Sieben JM, Duarte MME (2012) Methanol, ethanol and ethylene glycol electro-oxidation at Pt and Pt–Ru catalysts electrodeposited over oxidized carbon nanotubes. Int J Hydrogen Energy 37(13):9941–9947
10. Wang Y et al (2010) Electrocatalysis of carbon black- or activated carbon nanotubes-supported Pd–Ag towards methanol oxidation in alkaline media. Int J Hydrogen Energy 35(19):10087–10093
11. Peters TA et al (2017) Palladium (Pd) membranes as key enabling technology for pre-combustion CO_2 capture and hydrogen production. Energy Procedia 114:37–45
12. Arstad B et al (2006) Studies of self-supported 1.6 μm Pd/23 wt.% Ag membranes during and after hydrogen production in a catalytic membrane reactor. Catal Today 118(1–2):63–72
13. Mejdell AL et al (2009) Effects of CO and CO_2 on hydrogen permeation through a ~ 3 μm Pd/Ag 23 wt.% membrane employed in a microchannel membrane configuration. Sep Purif Technol 68(2):178–184

14. Amandusson H, Ekedahl L-G, Dannetun H (2000) The effect of CO and O_2 on hydrogen permeation through a palladium membrane. Appl Surf Sci 153(4):259–267
15. Mejdell AL et al (2010) The effect of heat treatment in air on CO inhibition of a ~ 3 μm Pd-Ag (23 wt.%) membrane. J Membr Sci 350(1–2):371–377
16. Peters TA, Stange M, Bredesen R (2011) On the high pressure performance of thin supported Pd–23%Ag membranes—evidence of ultrahigh hydrogen flux after air treatment. J Membr Sci 378(1–2):28–34
17. Svenum IH et al (2012) Adsorbate-induced segregation in a PdAg membrane model system: $Pd_3Ag(111)$. Catal Today 193(1):111–119
18. Ramachandran A et al (2010) Surface characterization of Pd/Ag23 wt% membranes after different thermal treatments. Appl Surf Sci 256(20):6121–6132
19. Wang D et al (2000) Enhanced rates of hydrogen absorption resulting from oxidation of Pd or internal oxidation of Pd-Al alloys. J Alloy Compd 298(1–2):261–273
20. Mejdell AL et al (2008) Hydrogen permeation of thin, free-standing Pd/Ag23% membranes before and after heat treatment in air. J Membr Sci 307(1):96–104
21. Zhang K et al (2012) A sorption rate hypothesis for the increase in H2 permeability of palladium-silver (Pd–Ag) membranes caused by air oxidation. Int J Hydrogen Energy 37(1):583–593
22. Vicinanza N et al (2018) New insight to the effects of heat treatment in air on the permeation properties of thin Pd77%Ag23% membranes. Membranes 8(4):92
23. Ali JK, Newson EJ, Rippin DWT (1994) Deactivation and regeneration of Pd–Ag membranes for dehydrogenation reactions. J Membr Sci 89(1–2):171–184
24. Yang L et al (2005) Changes in hydrogen permeability and surface state of Pd–Ag/ceramic composite membranes after thermal treatment. J Membr Sci 252(1–2):145–154
25. Christmann K, Ertl G, Schober O (1973) LEED intensities from clean and hydrogen covered Ni(100) and Pd(111) surfaces. Surf Sci 40(1):61–70
26. Felter TE, Sowa EC, Van Hove MA (1989) Location of hydrogen adsorbed on palladium (111) studied by low-energy electron diffraction. Phys Rev B 40(2):891
27. Behm RJ et al (1979) The structure of CO adsorbed on Pd(100): a leed and hreels analysis. Surf Sci 88(2):L59–L66
28. Morkel M, Rupprechter G, Freund H-J (2003) Ultrahigh vacuum and high-pressure coadsorption of CO and H2 on Pd(111): a combined SFG, TDS, and LEED study. J Chem Phys 119(20):10853–10866
29. Conrad H et al (1974) Adsorption of CO on Pd single crystal surfaces. Surf Sci 43(2):462–480
30. Conrad H, Ertl G, Latta EE (1974) Adsorption of hydrogen on palladium single crystal surfaces. Surf Sci 41(2):435–446
31. Noordermeer A, Kok GA, Nieuwenhuys BE (1986) A comparative study of the behaviour of the PdAg(111) and Pd(111) surfaces towards the interaction with hydrogen and carbon monoxide. Surf Sci 165(2–3):375–392
32. Guo X, Yates JT (1989) Dependence of effective desorption kinetic parameters on surface coverage and adsorption temperature: CO on Pd(111). J Chem Phys 90(11):6761–6766
33. Kok GA, Noordermeer A, Nieuwenhuys BE (1985) Effect of alloying on the adsorption of CO on palladium; A comparison of the behaviour of PdAg(111), PdCu(111) and Pd(111) surfaces. Surf Sci 152:505–512
34. Ma Y et al (2009) Formation, stability and CO adsorption properties of PdAg/Pd(1 1 1) surface alloys. Surf Sci 603(7):1046–1054
35. Greuter F et al (1986) Photoemission from H adsorbed on Ni(111) and Pd(111) surfaces. Phys Rev B 33(2):736
36. Andersen JN et al (1991) Surface core-level shifts as a probe of the local overlayer structure: CO on Pd(100). Phys Rev Lett 67(20):2822–2825
37. Surnev S et al (2000) CO adsorption on Pd(1 1 1): a high-resolution core level photoemission and electron energy loss spectroscopy study. Surf Sci 470(1–2):171–185
38. Fernandes VR et al (2014) Reduction behavior of oxidized Pd(100) and Pd75Ag25(100) surfaces using CO. Surf Sci 621:31–39
39. Eberhardt W, Louie SG, Plummer EW (1983) Interaction of hydrogen with a Pd(111) surface. Phys Rev B 28(2):465
40. Martin NM et al (2014) CO Adsorption on Clean and Oxidized Pd(111). J Phys Chem C 118(2):1118–1128
41. Rose MK et al (2002) Ordered structures of CO on Pd(1 1 1) studied by STM. Surf Sci 512(1–2):48–60
42. Mitsui T et al (2003) Hydrogen adsorption and diffusion on Pd(1 1 1). Surf Sci 540(1):5–11
43. Sautet P et al (2000) Adsorption and energetics of isolated CO molecules on Pd(111). Surf Sci 453(1–3):25–31
44. Blomberg S et al (2013) In situ X-ray photoelectron spectroscopy of model catalysts: at the edge of the gap. Phys Rev Lett 110(11):117601
45. Fernandes VR et al (2016) Reversed hysteresis during CO oxidation over Pd75Ag25(100). ACS Catal 6(7):4154–4161
46. Tang J et al (2019) Hydrogen adsorption and absorption on a Pd-Ag alloy surface studied using in-situ X-ray photoelectron spectroscopy under ultrahigh vacuum and ambient pressure. Appl Surf Sci 463:1161–1167
47. van Spronsen MA et al (2019) Dynamics of surface alloys: rearrangement of Pd/Ag(111) induced by CO and O2. J Phys Chem C 123(13):8312–8323
48. Toyoshima R et al (2012) Active surface oxygen for catalytic CO oxidation on Pd(100) proceeding under near ambient pressure conditions. J Phys Chem Lett 3(21):3182–3187
49. Greeley J, Mavrikakis M (2005) Surface and subsurface hydrogen: adsorption properties on transition metals and near-surface alloys. J Phys Chem B 109(8):3460–3471
50. Løvvik OM, Olsen RA (2003) Density functional calculations of hydrogen adsorption on palladium-silver alloy surfaces. J Chem Phys 118(7):3268–3272
51. Løvvik OM, Opalka SM (2008) Reversed surface segregation in palladium-silver alloys due to hydrogen adsorption. Surf Sci 602(17):2840–2844
52. Dong W, Hafner J (1997) H_2 dissociative adsorption on Pd(111). Phys Rev B 56(23):15396
53. Herron JA, Tonelli S, Mavrikakis M (2012) Atomic and molecular adsorption on Pd(111). Surf Sci 606(21–22):1670–1679
54. Mancera LA, Behm RJ, Groß A (2013) Structure and local reactivity of PdAg/Pd(111) surface alloys. Phys Chem Chem Phys 15(5):1497–1508
55. Ferrin P et al (2012) Hydrogen adsorption, absorption and diffusion on and in transition metal surfaces: a DFT study. Surf Sci 606(7):679–689
56. Wilke S, Scheffler M (1996) Potential-energy surface for H_2 dissociation over Pd(100). Phys Rev B 53(8):4926–4932
57. Rupprechter G et al (2004) Sum frequency generation and density functional studies of CO–H interaction and hydrogen bulk dissolution on Pd(1 1 1). Surf Sci 554(1):43–59
58. Paul JF, Sautet P (1996) Density-functional periodic study of the adsorption of hydrogen on a palladium (111) surface. Phys Rev B 53(12):8015–8027
59. Dong W et al (1996) Chemisorption of H on Pd(111): an ab initio approach with ultrasoft pseudopotentials. Phys Rev B 54(3):2157

60. Resch C et al (1994) Adsorption dynamics for the system hydrogen/palladium and its relation to the surface electronic structure. Surf Sci 316(3):L1105–L1109
61. Behm RJ, Christmann K, Ertl G (1980) Adsorption of hydrogen on Pd(100). Surf Sci 99(2):320–340
62. Rendulic KD, Anger G, Winkler A (1989) Wide range nozzle beam adsorption data for the systems H2/nickel and H2/Pd(100). Surf Sci 208(3):404–424
63. Mitsui T et al (2003) Dissociative hydrogen adsorption on palladium requires aggregates of three or more vacancies. Nature 422(6933):705–707
64. Ozawa N et al (2008) First principles study of hydrogen atom adsorption and diffusion on Pd3Ag(1 1 1) surface and in its subsurface. Surf Sci 602(4):859–863
65. Kuhn WK, Szanyi J, Goodman DW (1992) CO adsorption on Pd(111): the effects of temperature and pressure. Surf Sci 274(3):L611–L618
66. Gießel T et al (1998) A photoelectron diffraction study of ordered structures in the chemisorption system Pd{{111}}-CO. Surf Sci 406(1–3):90–102
67. Ma Y et al (2011) The interaction of CO with PdAg/Pd(111) surface alloys—a case study of ensemble effects on a bimetallic surface. Phys Chem Chem Phys 13(22):10741–10754
68. Crampin S (1993) Segregation and the work function of a random alloy: PdAg(111). J Phys 5(36):L443
69. Reniers F (1995) Use of matrix corrections in the calculation of surface composition of AgPd alloys in auger electron spectroscopy. Surf Interface Anal 23(6):374–380
70. Wouda PT et al (1998) STM study of the (111) and (100) surfaces of PdAg. Surf Sci 417(2–3):292–300
71. Walle LE et al (2012) Surface composition of clean and oxidized Pd75Ag25(100) from photoelectron spectroscopy and density functional theory calculations. Surf Sci 606(23–24):1777–1782
72. Løvvik OM (2005) Surface segregation in palladium based alloys from density-functional calculations. Surf Sci 583(1):100–106
73. Ruban AV et al (2007) Theoretical investigation of bulk ordering and surface segregation in Ag-Pd and other isoelectornic alloys. Phys Rev B 75(5):054113
74. Ropo M (2006) Ab initio study of the geometric dependence of AgPd surface segregation. Phys Rev B 74(19):195401
75. Ropo M, Kokko K (2005) Segregation at the PdAg(111) surface: electronic structure calculations. Phys Rev B 71(4):045411
76. Ruban AV, Skriver HL, Nørskov JK (1999) Surface segregation energies in transition-metal alloys. Phys Rev B 59(24):15990–16000
77. Hammer B, Hansen LB, Nørskov JK (1999) Improved adsorption energetics within density-functional theory using revised Perdew-Burke-Ernzerhof functionals. Phys Rev B 59(11):7413–7421
78. Greeley J, Nørskov JK, Mavrikakis M (2002) Electronic structure and catalysis on metal surfaces. Annu Rev Phys Chem 53(1):319–348
79. Perdew JP et al (1992) Atoms, molecules, solids, and surfaces: applications of the generalized gradient approximation for exchange and correlation. Phys Rev B 46(11):6671
80. White JA, Bird DM (1994) Implementation of gradient-corrected exchange-correlation potentials in Car-Parrinello total-energy calculations. Phys Rev B 50(7):4954
81. Vanderbilt D (1990) Soft self-consistent pseudopotentials in a generalized eigenvalue formalism. Phys Rev B 41(11):7892
82. Chadi DJ, Cohen ML (1973) Special points in the brillouin zone. Phys Rev B 8(12):5747
83. Coles BR (1965) The lattice spacings of nickel-copper and palladium-silver alloys. J Inst Met 48(9):346
84. Neugebauer J, Scheffler M (1992) Adsorbate-substrate and adsorbate-adsorbate interactions of Na and K adlayers on Al(111). Phys Rev B 46(24):16067
85. Bengtsson L (1999) Dipole correction for surface supercell calculations. Phys Rev B 59(19):12301–12304
86. Henkelman G, Jónsson H (2000) Improved tangent estimate in the nudged elastic band method for finding minimum energy paths and saddle points. J Chem Phys 113(22):9978–9985
87. Reuter K, Scheffler M (2003) First-principles atomistic thermodynamics for oxidation catalysis: surface phase diagrams and catalytically interesting regions. Phys Rev Lett 90(4):046103
88. Reuter K, Scheffler M (2003) Composition and structure of the RuO_2(110) surface in an O_2 and CO environment: Implications for the catalytic formation of CO_2. Phys Rev B 68(4):045407
89. Rogal J, Reuter K, Scheffler M (2007) CO oxidation at Pd(100): a first-principles constrained thermodynamics study. Phys Rev B 75(20):205433
90. Chase MW (1998) NIST-JANAF thermochemical tables. J Phys Chem Ref Data 9:1–1951
91. Lopez N, Nørskov JK (2001) Synergetic effects in CO adsorption on Cu-Pd(1 1 1) alloys. Surf Sci 477(1):59–75
92. Gallucci F et al (2007) The effect of mixture gas on hydrogen permeation through a palladium membrane: experimental study and theoretical approach. Int J Hydrogen Energy 32(12):1837–1845
93. Conrad H, Ertl G, Latta EE (1974) Coadsorption of hydrogen and carbon monoxide on a Pd (110) surface. J Catal 35(3):363–368
94. Johansson M et al (2010) Hydrogen adsorption on palladium and palladium hydride at 1 bar. Surf Sci 604(7–8):718–729
95. Dipojono HK et al (2010) A first principles study on dissociation and adsorption processes of H_2 on Pd_3Ag(111) surface. Jpn J Appl Phys 49:115702
96. Avouris P, Schmeisser D, Demuth JE (1982) Observation of rotational excitations of H_2 adsorbed on Ag surfaces. Phys Rev Lett 48(3):199–202
97. Sprunger PT, Plummer EW (1993) Interaction of hydrogen with the Ag(110) surface. Phys Rev B 48(19):14436–14446
98. Christmann K (1988) Interaction of hydrogen with solid surfaces. Surf Sci Rep 9(1–3):1–163
99. Mohammad AB et al (2007) A computational study of H2 dissociation on silver surfaces: the effect of oxygen in the added row structure of Ag(110). Phys Chem Chem Phys 9(10):1247–1254
100. Eichler A, Kresse G, Hafner J (1998) Ab-initio calculations of the 6D potential energy surfaces for the dissociative adsorption of H2 on the (100) surfaces of Rh, Pd and Ag. Surf Sci 397(1–3):116–136
101. Xu Y, Greeley J, Mavrikakis M (2005) Effect of subsurface oxygen on the reactivity of the Ag(111) surface. J Am Chem Soc 127(37):12823–12827
102. Nilekar AU et al (2010) Preferential CO oxidation in hydrogen: reactivity of core–shell nanoparticles. J Am Chem Soc 132(21):7418–7428
103. Eriksson M, Ekedahl LG (1998) Real time measurements of hydrogen desorption and absorption during CO exposures of Pd: hydrogen sticking and dissolution. Appl Surf Sci 133(1–2):89–97
104. Greeley J, Mavrikakis M (2003) A first-principles study of surface and subsurface H on and in Ni(1 1 1): diffusional properties and coverage-dependent behavior. Surf Sci 540(2–3):215–229
105. Canduela-Rodriguez G et al (2014) Thermodynamic study of benzene and hydrogen coadsorption on Pd(111). Phys Chem Chem Phys 16(43):23754–23768
106. Chizallet C et al (2011) Thermodynamic stability of buta-1,3-diene and But-1-ene on Pd(111) and (100) surfaces under H2 pressure: a DFT study. J Phys Chem C 115(24):12135–12149
107. Christmann K, Ertl G (1972) Adsorption of carbon monoxide on silver/palladium alloys. Surf Sci 33(2):254–270

108. Hoffmann FM (1983) Infrared reflection-absorption spectroscopy of adsorbed molecules. Surf Sci Rep 3(2–3):107–192
109. Duan Z, Henkelman G (2014) CO oxidation on the Pd(111) surface. ACS Catal 4(10):3435–3443
110. Ward TL, Dao T (1999) Model of hydrogen permeation behavior in palladium membranes. J Membr Sci 153(2):211–231
111. Xu L, Stangland EE, Mavrikakis M (2018) Ethylene versus ethane: a DFT-based selectivity descriptor for efficient catalyst screening. J Catal 362:18–24